Free growth and instability morphologies in directional melting of alloys

D. Benielli, N. Bergeon,* H. Jamgotchian, B. Billia, and Ph. Voge
Laboratoire Matériaux et Microélectronique de Provence (UMR CNRS 6137), Université d'Aix-Marseille, Faculté des Sciences et Techniques de Saint-Jérôme, Case 151, 13397 Marseille Cedex 20, France
(Received 18 January 2002; published 20 May 2002)

The dynamics of melting morphologies, namely, liquid droplets in the bulk solid and liquid dendrites due to morphological instability of the phase boundary, is observed *in situ* and in real time during directional melting of transparent succinonitrile-acetone alloys in a cylinder. Specific patterns are associated to grain boundaries. A model based on free growth but with time-dependent superheating is proposed for the lateral growth of the liquid inclusions. Contrary to what is largely believed, it is shown that free melting is not the mere reversal of free crystal growth, basically because solute diffusion is much lower in the solid, which imposes a boundary layer approach.

DOI: 10.1103/PhysRevE.65.051604 PACS number(s): 81.10.Fq, 47.20.Hw, 64.70.Dv, 68.08.−p

I. INTRODUCTION

It is a general observation in nature that, far from thermodynamic equilibrium, homogeneous systems are unstable and undergo the self-formation of structures [1]. Beside convection patterns in fluids, crystal growth morphologies have attracted increasing experimental and theoretical endeavor [2,3], motivated by both fundamental understanding of nonlinear physics and application in casting of structural materials. Comparatively, although the mastery of melting has become a critical issue for the tailoring of advanced materials, such as metallic superalloys [4] and the growth of large dislocation-free silicon crystals for electronics [5], melting morphologies until now have been rarely addressed [6–11], probably because no usable material is directly produced. Consequently, the knowledge of the basic physics still remains very incomplete, and in particular, demands to be substantiated by experiments. A further and direct motivation of the present work is the recent observation that the melting and thermal stabilization stages preparatory to directional solidification greatly effect the initial state on which growth is started [12].

Our aim is thus the deepening of the understanding of the dynamics of melting morphologies, namely, liquid droplets in the bulk solid and liquid dendrites due to morphological instability of the liquid-solid interface, on the basis of *in situ* and real-time observation carried out during directional melting of transparent succinonitrile-acetone alloys in a cylinder. By imposing a direction to the phase transformation, directional melting enables the precise study of fundamental aspects under well controlled conditions. The parallel with directional solidification is obvious. First, the alloy is molten by pulling the crucible through a thermal gradient G, and the control parameters of an experiment are G, pulling velocity V_P and initial solute concentration C_0. Second, for given C_0 and G, the planar liquid-solid interface can be destabilized by increasing V_P beyond a critical value, thus giving rise to cellular microstructures [8,9]. Yet, there is a major difference: since it is linked to solute diffusion in the solid, constitutional superheating can easily build up and is large in the solid well before morphological instability that is dominated by solute diffusion in the liquid [7,9,11], which is contrary to solidification where constitutional supercooling in the melt also depends on solute diffusion in the liquid [13]. The most striking outcome is the nucleation and visible growth of liquid droplets in the superheated solid, which is quantitatively analyzed in the following.

The experimental setup is described in detail in Ref. [14] so that only specific features of interest for present purposes are briefly presented. The fully solid succinonitrile-acetone alloy ($C_0 = 0.08$ and 0.2 wt %) of 15 cm in length is contained in a cylindrical glass crucible (inner diameter $\Phi = 10$ mm), with a flat pyrex window at the bottom and closed by an immersed lens at the top. The applied temperature gradient $G = 30$ K/cm and directional melting is achieved by translating the sample upwards at velocity V_P (= 20 and 30 mm/s). Bright-field images are obtained by direct observation from the top using the light transmitted through the entire sample length. Basically, droplets show up with the contour of the largest horizontal cross section (see Fig. 5), and the microstructure induced at the liquid-solid interface by morphological instability appears mostly through contrasts associated to the cap regions (see Fig. 2). It should be stressed that directional melting is achieved on a solid alloy obtained by upward directional solidification with a solid-liquid interface that can be made either smooth or cellular. In the former case no microsegregation of acetone is embedded in the solid whereas, in the latter case, the subsequent melting takes place from the end of the microsegregation left by the microstructure created in the solidification process, which is not really desirable as the interpretation of the melting morphologies is then rendered more complex. In practice, the observed phenomena fall into two categories that will be treated consecutively: melting morphologies resulting from the instability of the liquid-solid interface and liquid droplets in the superheated solid, that is sometimes referred to as premelting phenomenon [6].

II. MELTING MORPHOLOGIES AT THE SOLID-LIQUID INTERFACE

The advancement of the analysis of the morphological stability of a planar liquid-solid interface in directional melt-

*Electronic address: bergeon@L2MP.u-3mrs.fr

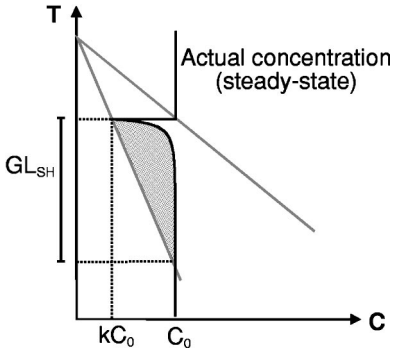

FIG. 1. Solute profile in the solid during steady-state directional melting superposed to the equilibrium phase diagram. In this figure, the experimental control parameters lead to the formation of a constitutionally superheated (SH) zone (gray area), whose length is denoted by L_{SH}, characterized by an actual temperature higher than the equilibrium temperature. In this region, coexistence of solid and liquid is possible. G: thermal gradient.

ing of a binary alloy [7,11] parallels that for directional solidification [14,15]. By solving the equation of solute, diffusion in the solid and solute balance at the interface during steady state melting, the concentration profile in the solid can be determined, and the thermodynamic stability of the solid phase can be analyzed by superposing it on the phase diagram (Fig. 1). It follows that a region of constitutional superheating is present ahead of the melting interface when the melting velocity V is greater than a critical value V_{CS},

$$V > V_{CS} = kD_S G/[mC_O(k-1)], \tag{1}$$

with k the solute segregation coefficient, m the liquidus slope, and D_S the solute diffusion coefficient in the solid. By analogy with solidification, it might seem reasonable to suppose that the planar melting front is then morphologically unstable.

Yet, it is long known from experiments that constitutional superheating can exist without implying morphological instability [6,8], which invalidates the constitutional superheating criterion. The explanation came from the linear stability analysis [7,9,11] that pointed out that solute diffusion in the liquid phase has a drastic stabilizing effect. Indeed, the criterion for morphological instability in directional melting now reads [11]

$$V > V_{MI} = (kD_S + D_L)G/[mC_O(k-1)], \tag{2}$$

with D_L the solute diffusion coefficient in the liquid, which is much larger than D_S. For most alloy systems, $kD_S/D_L \ll 1$, so that solute diffusion in the solid can be neglected in criterion (2), that reduces to

$$V > V_{MI} = D_L G/[mC_O(k-1)]. \tag{3}$$

Different structures resulting from morphological instability of the melting front have been observed in our experiments, which actually depend on local experimental conditions rather than on the global criterion (3). Indeed, there is always significant buoyancy-driven fluid flow in the preparatory directional solidification step [12,13], which, in particular, results in acetone macrosegregretion along the growth direction and at the solid-liquid interface. Therefore, although the local concentration C_{loc} in the solid at the interface is not accessible in experiment, it is condition (3) with C_{loc} instead of C_O, which is quantitatively meaningful. Accordingly, it is the type of microstructure that is observed that in practice provides a qualitative measure of the local degree of instability.

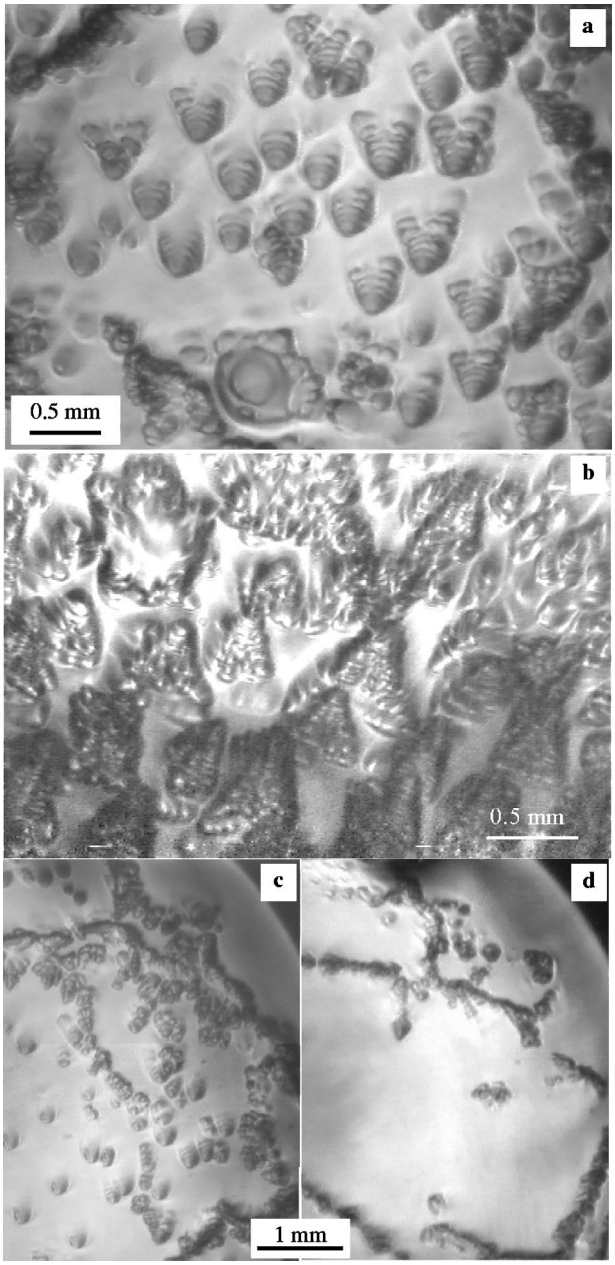

FIG. 2. (a),(b) Arrays of melting dendrites in a grain. (c) Less prominent dendrites inside grains, 12 mm below Fig. 2(a). (d) Melting morphologies confined to grain (sub-)boundaries, 37 mm below Fig. 2(a). Direct observation, $C_0 = 0.2$ wt % acetone, $G = 30$ K/cm, $V_P = 30$ μm/s, melting after solidification at 0.4 μm/s.

For instance, for melting experiments at $V_P = 30$ μm/s and $G = 30$ K/cm on the succinonitrile-acetone (0.2 wt %)

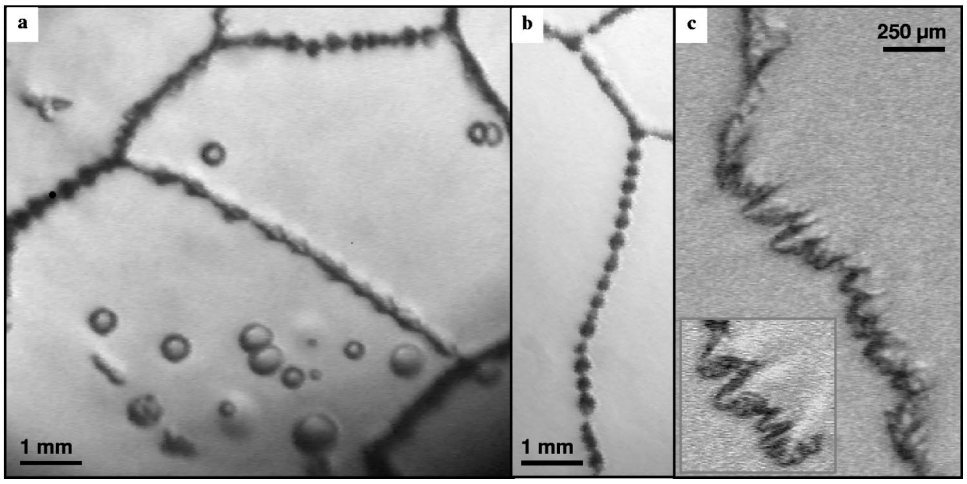

FIG. 3. Close-up observation of melting morphologies localized at grain boundaries and liquid droplets in the superheated region of grains. Direct observation, $C_0 = 0.08$ wt % acetone, $G = 20$ K/cm, $V_P = 30$ μm/s, melting after solidification at 0.4 μm/s.

sample after solidification at slow rate (0.4 μm/s), arrays of melting dendrites first form in the grains (Fig. 2), which means that the local solute concentration is much higher than that corresponding to the critical velocity $V_{MI} = V_P$ in Eq. (3), namely, $C_{loc} = 0.05$ wt % with $k = 0.1$, $m = -2.8$ K/wt %, and $D_L = 1.3 \times 10^{-5}$ cm^2/s. Symmetric to solidification cells and dendrites that are directed towards the liquid in solidification, the tips of the liquid dendrites are penetrating into the solid while the bodies are separated from one another by a layer of smooth interface, in the same way as the eutectic layer that commonly terminates the liquid grooves in between solidification dendrites. Their orientation with respect to the liquid-solid interface is determined by the anisotropy of solid succinonitrile that favors growth in ⟨100⟩ direction, and the orientation of the grains they occupy. As sidebranches are visible on 3 or 4 fins, these dendrites are definitely three dimensional (3D). Farther on in directional melting, the dendrites become less pronounced while the proportion of smooth interface increases, and finally they disappear from the interior of the grains when C_{loc} is too low, as exemplified in Figs. 2(c) and 2(d), respectively, taken 12 and 32 mm below Fig. 2(a). It follows from such an evolution that the longitudinal acetone macrosegregation left by solidification is closer to the complete-mixing limit with characteristic Scheil profile in the solid, $C_S = kC_O(1 - f_S)^{k-1}$ with f_S the solid fraction, than to the limit of diffusive transport in the melt, for which there would be a plateau at C_O and thus continuation of the melting pattern.

For experiments at $V_P = 30$ μm/s and $G = 20$ K/cm performed with $C_0 = 0.08$ wt % acetone after slow solidification at 0.4 μm/s, for which the degree of instability is comparatively weaker, melting morphologies are most of the time confined to grain boundaries and sub-boundaries (Fig. 3) as in Fig. 2(d), which confirms that defects in the solid locally enhance melting [18]. Even when they are hardly visible by themselves, sub-boundaries are made apparent by the alignment of structures that eventually decorate them. Indeed, melting at grain boundaries in general breaks out into chains of liquid ''pockets'' that follow the motion imposed by directional melting [Figs. 3(a) and 3(b)]. On inclined grain boundaries, we otherwise observe 2D patterns [Fig. 3(c)] that are very much alike the seaweed and dendritic structures that form in the solidification of thin samples [19]. Figure 4 schematically explains the lateral propagation of such 2D instabilities seen in the top view of the interface at two successive times. As we previously noticed in directional solidification of succinonitrile-acetone alloys [20], grain boundaries act as finite preexisting perturbations but, at that time, it is the triple-junction line that is at the forefront of the process of phase change, which suggests that the origin of the 2D character of the patterns can be attributed to the morphological instability of that leading line whose melting point is presumably lowered due to higher local solute concentration.

When the preparatory solidification is realized at a pulling rate high enough to get morphological instability at the solid-

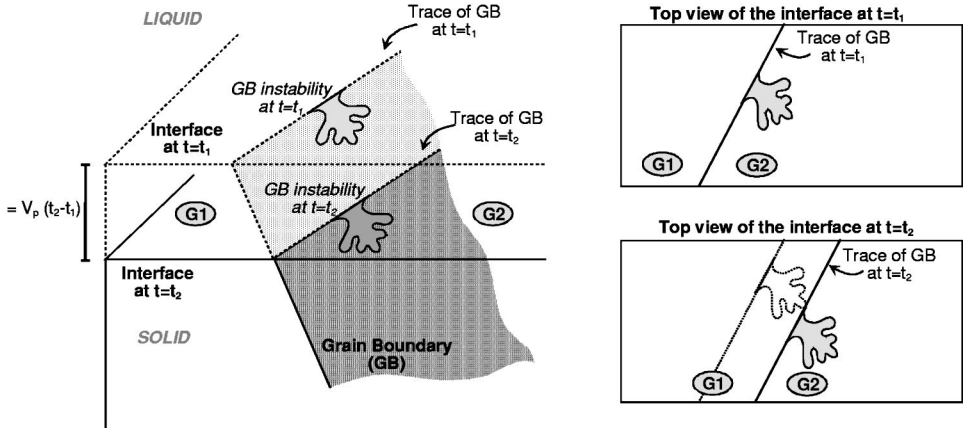

FIG. 4. Schematic representation of the images obtained at two successive times by direct observation from the top of a dendrite-like morphology attached to an inclined grain boundary.

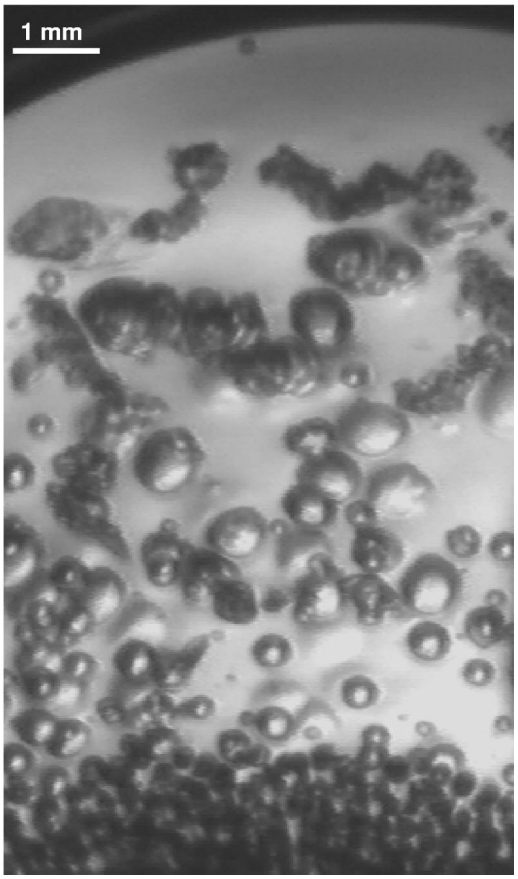

FIG. 5. Evolution of the melting morphology from the center to the crucible border in the case of preparatory solidification with central cellular pattern. Direct observation, $C_0=0.08$ wt % acetone, $G=20$ K/cm, $V_P=30$ μm/s, melting after solidification at 2 μm/s.

liquid interface, e.g., 2 μm/s instead of 0.4 μm/s for the same 0.08 wt % acetone sample, the melting morphology evolves when going from the center to the crucible border (Fig. 5). This is because convection due to radial thermal gradient induces solute accumulation at the center of the interface and focus-type localization of the cellular microstructures [see Fig. 2(b) in Ref. [17]]. Then, in the central part (bottom of Fig. 5) the melting pattern follows the acetone microsegregation left by the array of solidification cells and, in the external region where the solidification front was smooth, numerous liquid droplets are observed in the superheated solid.

III. DROPLETS IN THE SUPERHEATED SOLID

As previously mentioned, the onset of morphological instability of the planar melting front is situated far above that of constitutional superheating of the solid. However, in the interval the possibility of nucleation and growth of the liquid phase in the superheated region should be considered. For instance, Woodruff and Forty [6] and Verhoeven and Gibson [8] report interesting phenomena of local melting in the solid ahead of the interface, observed in thin films of sodium-potassium solutions and in bulk Sn-Bi and Sn-Sb alloys, respectively.

The length L_{SH} of the superheated solid is determined by the intersection between the actual temperature and equilibrium temperature profiles (Fig. 1). In steady-state directional melting, the solutal length $l_S=D_S/V_P$ is usually very short due to low solute diffusion in the solid. It follows that the intersection defining L_{SH} is located at the equilibrium temperature $T_{eq}(C_0)$ given by the solidus of the phase diagram, on the plateau corresponding to homogeneous solid at concentration C_O. Under these conditions, L_{SH} is given by

$$L_{SH}=mC_O(k-1)/(Gk), \tag{4}$$

which does not depend on the pulling rate V_P but only on thermal gradient and solute concentration.

As no precise value of the diffusion coefficient of acetone in solid succinonitrile is available, we follow Kirkaldy *et al.* [21] and consider reasonable to take $D_L/D_S\sim 100$. Then, l_S varies from 0.9 to 0.3 μm for pulling rates between 10 and 30 μm/s, which is much smaller than the values given by Eq. (4) for L_{SH}, namely, $L_{SH}=1.0$ mm for $C_0=0.08$ wt % and $G=20$ K/cm and $L_{SH}=1.7$ mm for $C_0=0.2$ wt% and $G=30$ K/cm, which validates the aforementioned approximation.

A. Observation

Owing to the large depth of focus of our setup in bright-field observation in the growth direction, the droplets nucleated in the core of the solid ahead the melting interface have been observed *in situ* and their growth analyzed until their disappearance when they coalesce with the bulk liquid.

Figure 6 illustrates the observation of a droplet at different stages of its evolution. Figure 6(a) corresponds to its first observation, when the droplet size has reached the minimum visible size. It is worth noting that it is not exactly the nucleation time. The droplet increases in size with time [Fig. 6(b)], and finally emerges at the interface where it vanishes into the bulk liquid [Fig. 6(c)]. Actually, the droplet grows in an environment that is continuously changing under the joint action of directional pulling at V_P, which translates the temperature profile and melting interface downwards together, and temperature gradient zone melting (TGZM) [22] that provides an additional speed to the droplet migration towards the interface.

The TGZM process is schematically described in Fig. 7. In a droplet subjected to a temperature gradient, a concentration gradient exists in the liquid between the bottom (T_2,C_2) and the top (T_1,C_1) that drives solute diffusion from cold to hot. An increase of the solute concentration at the top, from C_1 to C_1', and a decrease at the bottom, from C_2 to C_2', simultaneously result. As the actual temperature profile in the droplet, which is imposed by the external thermal gradient, does not change, the representative point of the top (T_1,C_1') is on the phase diagram shifted to the right into the liquid, that results in melting at the droplet hot end. Symmetrically, the shift of the representative point of the bottom (T_2,C_2') into the solid induces solidification at the droplet cold end. Globally, the effect of TGZM is thus the migration of the

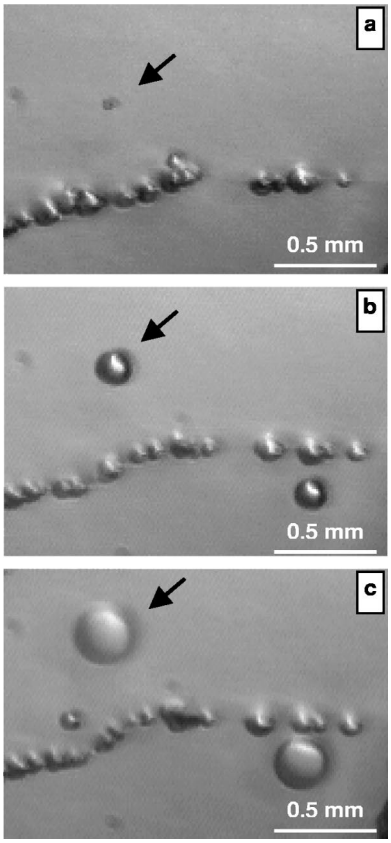

FIG. 6. Different stages of a droplet growth. (a) Just visible a little after the nucleation, (b) growth, 5 s later than (a), (c) emergence at the front of directional melting, 10 s later than (a). Direct observation, $C_0=0.08$ wt % acetone, $G=20$ K/cm, $V_P=30$ μm/s, melting after solidification at 0.4 μm/s.

droplet up the temperature gradient, at a rate V_{mig} that was estimated by Tiller [23]

$$V_{mig}=-G_L D_L/[mC_L(k-1)], \tag{5}$$

with G_L and C_L the thermal gradient and average solute concentration in the liquid droplet.

The number of droplets varies with experimental parameters. As already noticed by Verhoeven and Gibson [8], it increases with pulling rate. The lifetime τ of a droplet, defined as the duration from the moment it becomes visible to its disappearance at the interface, can be used to get an estimate of its nucleation depth Z_i by using the global rate of droplet motion with respect to the melting interface $V_d=V_P-V_{mig}$. As the migration rate depends on C_L that is changing all along the droplet motion, the rate V_d is a function of Z so that the lifetime τ is related to Z_i by

$$\tau=\int_0^{Z_i} dZ/V_d(Z) \tag{6}$$

with

$$V_d(z)-V_P=\frac{GD_L}{m(k-1)C_L} \tag{7}$$

$$=\frac{GD_L}{m(k-1)(C_O+GZ/|m|)}. \tag{8}$$

The calculated lifetime as function of the nondimensional nucleation depth $f=Z_i/L_{SH}$ for the considered concentrations of 0.08 and 0.2 wt % acetone is drawn in full and dashed lines in Fig. 8(a). For each acetone concentration, the lifetime τ has been measured for a large number of droplets, and also a value of the depth f associated to τ is measured by using the curves in Fig. 8(a). It is worth noting that a measure does not exactly correspond to the real lifetime as it begins when the droplet is visible and not when it nucleates. The resulting distributions of the droplet fraction (number of droplets nucleated in an interval of depth f divided by the total number of counted droplets) are given in Fig. 8(b) in white ($C_O=0.2$ wt %) and black ($C_O=0.08$ wt %) squares. It results that the droplet nucleation commences at $f\sim0.6$, exhibits a peak at $f\sim0.4$ and ceases at $f\sim0.2$, which is characteristic of heterogeneous nucleation starting at a critical superheating, and increasing rapidly before declining due to the exhaustion of the nucleation sites [24] that are probably tiny spots where acetone has accumulated. Furthermore, as nondimensional superheating is given by $1-f=(L_{SH}-Z_i)/L_{SH}$, it stems from Fig. 8(b) that the critical superheating for heterogeneous nucleation is at most of the order of 1 K, which is much less than the stability limit against homogeneous nucleation for a superheated crystal [25] that is of

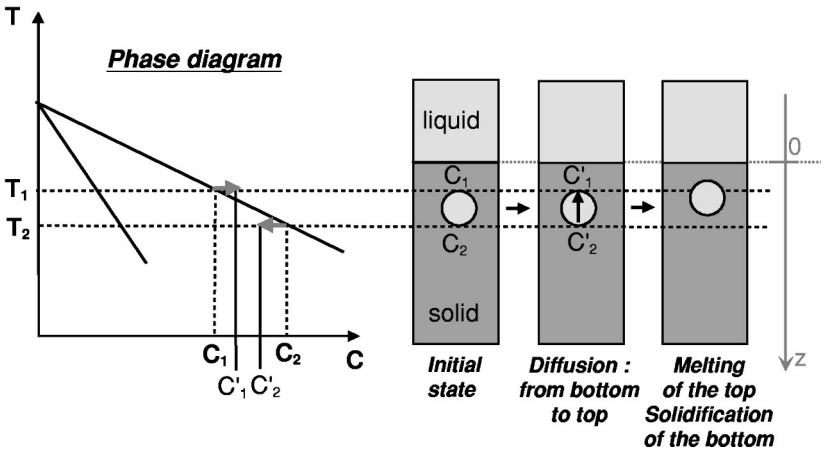

FIG. 7. Sketch of the TGZM process. The concentration gradient resulting from the temperature gradient induces solute diffusion inside the droplet that in turn causes melting at the droplet hot end (top) and solidification at the cold end (bottom).

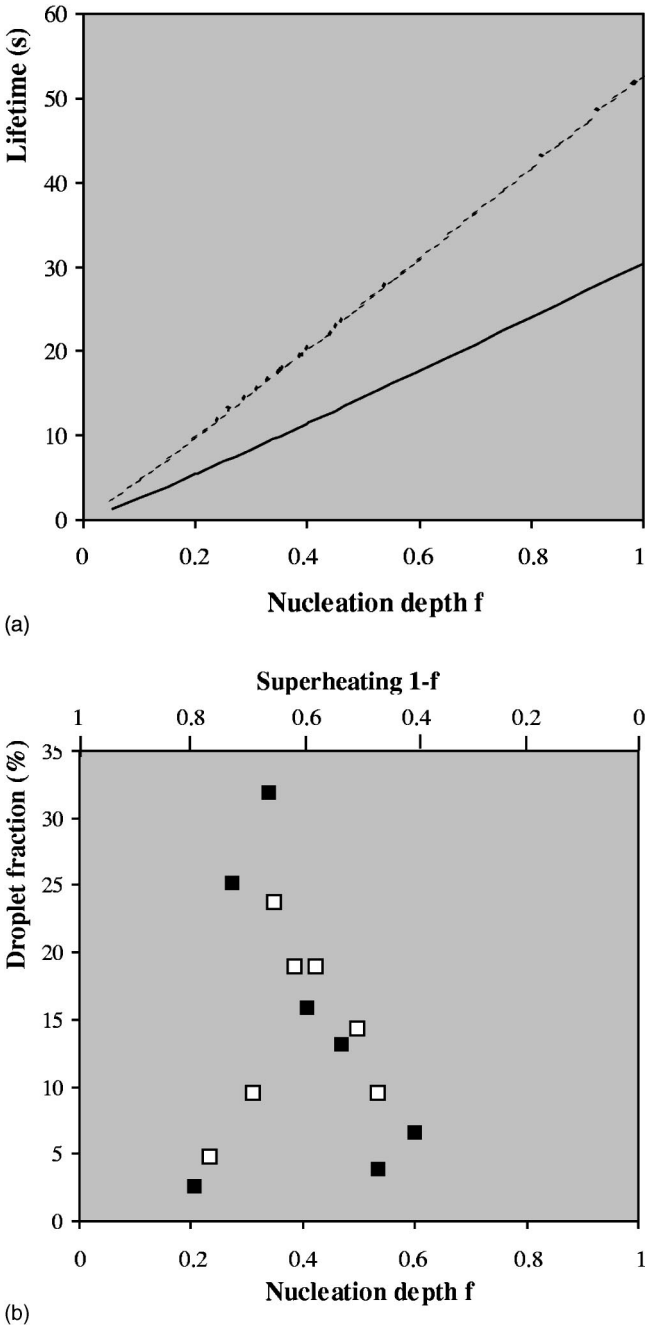

FIG. 8. (a) Calculated lifetime (sec) as function of the nucleation depth f for the two considered acetone concentrations, 0.08 and 0.2 wt % in full and dashed lines. (b) Histograms of experimental lifetimes for $C_0=0.2$ wt % (full squares) and $C_0=0.08$ wt % (open squares).

the order of one-tenth of the melting temperature ($=30$ K for succinonitrile). Considering that the first instants of droplet existence are not taken into account, which in practice somewhat shifts the distributions to lower f in Fig. 8(b), the present results are consistent with the observations of Verhoeven and Gibson [8] who found that the zone of liquid and solid coexistence extends from the interface to a depth f ranging from 0.5 to 0.75.

It is of value to note that in a population of droplets, the development of bumps (Fig. 9) is observed on a significant fraction of them, which might be tentatively attributed to the morphological instability of the liquid-solid interface. This point would yet deserve further clarification as, in particular, the droplets of largest cross section in general do not have bumps.

B. Modeling of the lateral growth of droplets

Taking advantage of *in situ* and real-time observation, growth of droplets has been studied through measurements of the droplet diameter $2R$ as function of time. Examples of such measurements are given in Fig. 10. Experimentally, the measured diameters correspond to the lateral growth of the largest horizontal cross section of the droplet which, although its temperature increases with time as the front of directional melting is approaching, is an isothermal plane that henceforth will be taken as the reference plane Z_d. Indeed, as heat diffuses much faster than solute, the thermal effects induced by the phase change can be neglected and the temperature throughout the system is determined by the applied thermal gradient $G(>0)$, which corresponds to the commonly used frozen temperature approximation of in the literature [26],

$$T=T_O-G(Z-Z_O)+GV_P(t-t_O), \tag{9}$$

in a frame attached to the crucible, with T_O the liquidus temperature for solute concentration C_O and Z_O the vertical position of the isotherm T_O at the time t_O at which the droplet appears. The rate of the droplet interface in the horizontal plane of largest cross section is denoted $V_R=dR/dt$.

The formation of liquid droplets in the solid is due to the existence of a region of superheated solid where the coexistence of liquid and solid is possible. Because of the relative motion of the droplets towards the liquid-solid interface, due to the conjugate action of directional melting and TGZM the problem has only cylindrical symmetry, that is the first major contradistinction with classical free growth that possesses spherical symmetry [27,28]. Thus, we should consider the growth dynamics of a liquid droplet with cylindrical symmetry surrounded by solid, located in this superheated zone. Its nucleation occurs at a distance Z_i in the solid, at a temperature given by Eq. (9). Local equilibrium is assumed at the interface during the whole growth so that the solid and liquid concentrations at the droplet interface, $C_S(T)$ and $C_L(T)$, lie respectively on the solidus and liquidus lines of the phase diagram, with $C_S(T)=kC_L(T)$.

In cylindrical coordinates attached to the droplet, with the vertical z axis in the direction of directional melting at V_p and the origin $(r=0,z=0)$ at the center of the largest horizontal cross section of the droplet, the solute fields in the liquid droplet and in the solid around it, $C_L(r,z)$ and $C_S(r,z)$, satisfy the following equation of diffusion

$$\frac{\partial C_i}{\partial t}-V_{mig}\frac{\partial C_i}{\partial z}=D_i\left(\frac{\partial^2 C_i}{\partial r^2}+\frac{1}{r}\frac{\partial Ci}{\partial r}+\frac{\partial^2 C_i}{\partial z^2}\right),$$

$$i=L \text{ or } S. \tag{10}$$

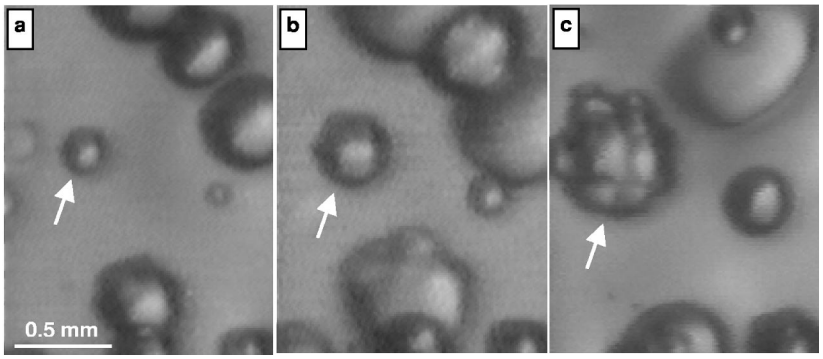

FIG. 9. Development of bumps probably showing the morphological instability of the liquid-solid interface of the droplet. Direct observation, $C_0 = 0.08$ wt % acetone, $G = 20$ K/cm, $V_P = 20$ μm/s, melting after solidification at 0.4 μm/s.

In Eq. (10), the time derivative $\partial C_i / \partial t$ not only contains the concentration variation due to the fact that the evolution (growth, shrinkage or a combination) of a droplet is by nature time dependent. Heating by directional melting at GV_P and caused by the droplet migration at V_{mig} up the temperature gradient G also contribute to $\partial C_i / \partial t$, as the solute fields must satisfy the boundary conditions of local equilibrium at any point on the solid-liquid interface ϕ.

$$C_L|_\phi = C_O + \frac{G}{m}[(Z_O - Z_{d,O} - z) + (V_P - V_{mig})(t - t_O)], \tag{11}$$

$$C_S|_\phi = kC_O + \frac{G}{n}[(Z_O - Z_{d,O} - z) + (V_P - V_{mig})(t - t_O)], \tag{12}$$

with $Z_{d,O}$ the droplet vertical position at t_O and n the solidus slope.

The second major difference with classical free growth is the mere consequence of the TGZM process. Indeed, it should be recognized that the evolution of the vertical dimension H of the droplet is directly related to the difference of interface velocity between the melting hot end and solidifying cold end, in a way similar to that described by Allen and Hunt in their study of the migration of dendrite secondary arms in directional solidification [29], whereas the driving force for free growth is the distance from thermodynamic equilibrium, given by the lever rule. As in direct observation from the top we have no access to the vertical dimension, this point will not be further pursued.

In order to model the growth of the largest cross section of the droplet that is what is observed as two-dimensional (2D) growth, we adopt an approach inspired by that used by Brener to describe the growth of the cross section of three-dimensional dendrites [30]. Indeed, when the derivatives with respect to z can be neglected for the solid, Eq. (10) reduces to a 2D equation that describes the free growth of an isothermal cross section controlled by solute diffusion from

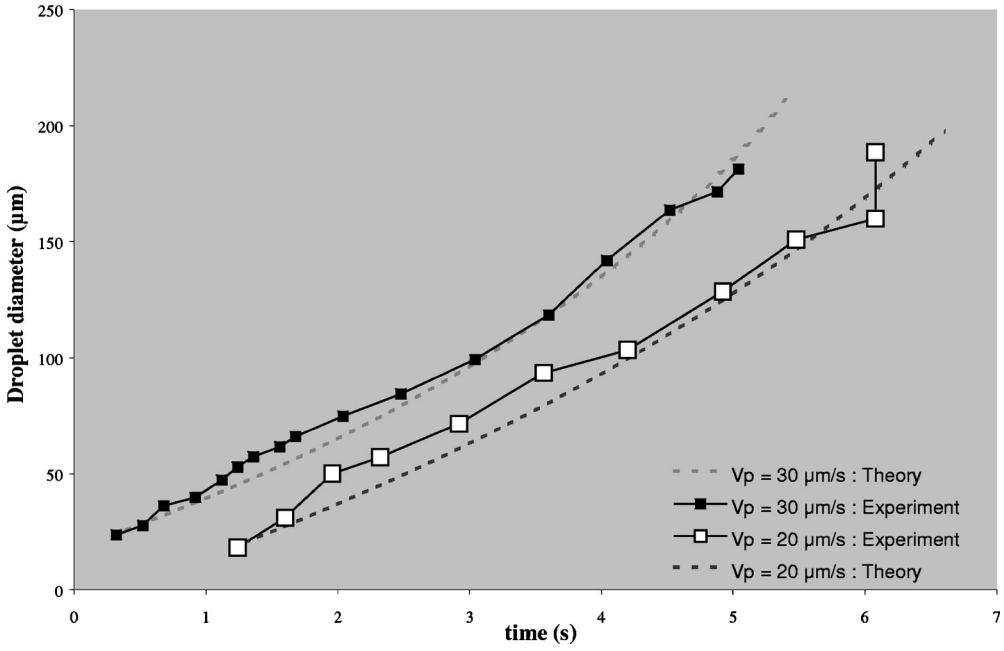

FIG. 10. Typical examples of the radial growth of droplets, represented by the variation of the droplet diameter (μm) versus time (sec). Experimental curves (solid lines) are compared to theoretical modeling (dashed lines) for two different pulling rates. $C_0 = 0.08$ wt % acetone, $G = 20$ K/cm, melting after solidification at 0.4 μm/s, $\delta = 0.36$ μm.

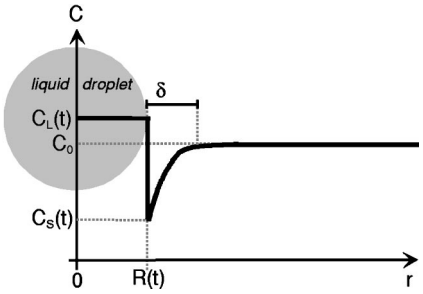

FIG. 11. Schematic representation of the solute concentration profile in the solid surrounding a liquid droplet, in and about the plane of maximum horizontal cross section, whose radius is *R*. The characteristic decay length δ is of the order of the solutal length, smaller than the droplet radius.

the solid to the liquid through a diffusion boundary layer (Fig. 11). In other words, droplet growth in this limit is split into two independent components: one-dimensional growth in *z* controlled by TGZM and free growth of the 2D cross section at $z=0$.

The last subtlety to notice is that, as the droplet moves up to higher temperature, the distance from thermodynamic equilibrium, measured by the dimensionless superheating $\Delta=[C_O-C_S(T)]/[C_L(T)-C_S(T)]$, increases continuously from about zero at nucleation to unity when the liquid-solid interface is met and C_O becomes the liquidus concentration $C_L(T)$.

Assuming that the *z* terms are negligible (to be verified) and, although we know that at long times Δ becomes unity, under the condition that the time derivative can be omitted for the sake of a tractable first order approach, Eq. (10) leads to

$$\partial^2 C(r,0)/\partial r^2 + r^{-1}\partial C(r,0)/\partial r = 0. \tag{13}$$

The solution of Eq. (13) is

$$C(r,0) = A + B\ln(r). \tag{14}$$

The boundary conditions are simply given by local equilibrium at the droplet interface [$C=C_S(T)$ for $r=R$] and the concentration C_O at a finite distance δ from the interface. This last condition implies $C=C_O$ for $r=R+\delta$, as it was previously observed in transmission ultraviolet microscopy investigation of melting in thin film of potassium-sodium alloys [6]. This approach can be compared to the definition of limit boundary layers for convection problems. Equation (14) then becomes

$$C(r,0) = C_O - [C_O - C_S(T)]\frac{1-\ln(r/R)}{\ln(1+\delta/R)}. \tag{15}$$

Derivation of Eq. (15) gives

$$\left.\frac{\partial C(r,0)}{\partial r}\right|_R = \frac{C_O - C_S(T)}{R\ln(1+\delta/R)}. \tag{16}$$

Solute conservation at the interface at, and about, $z=0$ is written as

$$[C_L(T) - C_S(T)]V_R = D_S \partial C(r,0)/\partial r|_R \tag{17}$$

because the solute field in the liquid does not depend on r as long as the droplet velocity relative to the liquid-solid interface of directional melting is not too fast (see, e.g., Tiller [23]). Indeed, the solute field inside the droplet then remains equal to $C_S(T)/k - Gz/m$ that matches with the condition of local equilibrium at the droplet interface, whatever be its shape. Actually, the horizontal solute gradient in the liquid, if any, is the mere consequence of the departure from linearity of the solute field in the droplet. This is the case when the solute balance in the liquid, Eq. (10), can no longer be reduced to $D_L \partial^2 C_L/\partial z^2 = 0$, which may occur after some time of the droplet growth if $(V_P - V_{mig})H/D_L > 1$. It is assumed that, even if this condition is satisfied, Eq. (17) remains a good approximation.

Introducing Eq. (16) in Eq. (17)

$$dR = \frac{D_S k[C_O - C_S(T)]}{(1-k)C_S(T)R\ln(1+\delta/R)}dt \tag{18}$$

$$= \frac{D_S \Delta}{R\ln(1+\delta/R)}dt. \tag{19}$$

For $\delta \ll R$, Eq. (19) becomes

$$dR = \frac{D_S k[C_O - C_S(T)]}{(1-k)C_S(T)\delta}dt = \frac{D_S \Delta}{\delta}dt. \tag{20}$$

The numerical integration of Eq. (20) is carried out by using the following difference equation

$$R(t_{n+1}) = R(t_n) + \Delta R(t_n), \tag{21}$$

$$\Delta R(t_n) = \frac{D_S k}{\delta(1-k)}\left(\frac{C_O}{C_S(T)} - 1\right)\Delta t, \tag{22}$$

with $R(t_1)=R_1$ as the first experimental radius measured at $t=t_1$,

$$C_S(t_{n+1}) = C_S(t_n) + kGV_d\Delta t/m, \tag{23}$$

and $C_S(t_1+\tau) = kC_O$.

The theoretical growth of the droplet diameter is shown with dashed lines in Fig. 10 for the value of δ that gives the best fit. The droplet diameter increases faster than the linear one because Δ is an increasing function of time and dR/dt is proportional to Δ [see Eq. (20)]. It is gratifying that an excellent agreement with experimental data is obtained for a value of δ such that $\delta \sim D_S/V_R < R$ as this is consistent with the boundary layer approach adopted in modeling. In contradistinction with free growth of a solid where, as it is much smaller than the solutal length D_L/V_R, the crystal radius gives the length scale, two characteristic lengths have to be taken into account simultaneously when addressing free growth in melting: the droplet radius, as it is still the shape parameter, and the solutal length in the solid phase that is now the shortest length in the problem over which acetone is transported from the bulk solid at C_O to feed the lateral growth of the droplet (Fig. 11).

The previous calculations have been performed under the hypothesis that only the r terms in Eq. (10) have to be considered for the solid phase, in order to get Eq. (13). This can now be justified by an order-of-magnitude analysis. As the thermal environment in which the droplet is moving is changing at velocity V_d, the order of magnitude of $\partial C/\partial t - V_{mig}\partial C/\partial z$ is $V_d kG/m$, that of $D_S\partial^2 C/\partial z^2$ is $D_S(kGH/m)/H^2$, and that of $D_S\partial^2 C/\partial r^2$ is $D_S[C_O - C_S(T)]/\delta^2$. Thus,

$$\left[\frac{\partial C}{\partial t} - V_{mig}\frac{\partial C}{\partial z}\right] \Bigg/ \left[D_S\frac{\partial^2 C}{\partial r^2}\right] = O\left(\frac{V_d kG\,\delta^2}{mD_S(C_O - C_S(T))}\right),$$

which is always less than 10^{-3} in the range of our measurements during the whole droplet motion, from which it follows that $\partial C/\partial t - V_{mig}\partial C/\partial z$ is indeed negligible in Eq. (10). The same thing holds for $D_S\partial^2 C/\partial z^2$ that is even smaller as $[\partial C/\partial t - V_{mig}\partial C/\partial z]/[D_S\partial^2 C/\partial r^2] = \{V_d H/D_S\} \gg 1$. The orders of magnitude are evaluated at each time step using the instantaneous values of V_d and C_S given by Eqs. (7) and (23), respectively.

IV. CONCLUSION

By means of sharp *in situ* and real-time observation during directional melting of transparent succinonitrile-acetone alloys in a cylinder, the melting morphologies, namely, liquid droplets in the bulk, solid, and liquid dendrites due to morphological instability of the phase boundary, have been brought to light. Although dendrites were observed a few times in free melting, no observation of arrayed-dendrite growth in directional melting was, to our knowledge, reported in the literature. Early melting and specific patterns are associated to grain boundaries. In order to explain the dynamics of the lateral growth of liquid droplets in the constitutionally superheated solid, a model based on the free-growth approach is proposed, which possesses two distinctive features: superheating is time dependent due to directional heating and droplet migration by TGZM, and a boundary layer approach for solute transport in the solid around the droplet, imposed by the fact that solute diffusion is slow in the solid, definitely prevents to describe free melting as the direct reversal of free crystal growth.

Further studies of melting phenomena would be more helpful especially to get complementary information on the phenomena. First, it would be interesting to carry out experiments in the limit of diffusive transport of solute in the liquid that, for our bulk cylindrical samples, imposes to work in the absence of gravity at least for preparatory directional solidification, so it is already planned to pursue our investigation on board of the International Space Station as soon as it becomes available. One could also think to thin-film experiments but then caution should be taken to avoid artifacts, such as parasitic heterogeneous nucleation of droplets at the glass walls. Second, simultaneous observation from the side is desirable, which among other things would give complete information on the droplet shape. For our experimental setup, this is presently far beyond the optical resolution we have in observation from the side.

Finally, this study provides critical data that call for new efforts to advance theoretical modeling and numerical simulation which, in particular, by enabling the resolution of the full time-dependent equations, would get rid off the limiting assumptions used in our approach. Thus they timely provide deeper, if not definitive, understanding of the formation and the dynamics of the melting morphologies.

ACKNOWLEDGMENTS

This study was carried out within the DECLIC project of the Center National d'Etudes Spatiales, and was also supported by the European Space Agency (''CETSOL'' MAP No. 14313). The authors express their gratitude to the other members of the ''Modes et formes de croissance'' team at L2MP, as well as to K. Kassner and R. Ghez for enlightening discussions.

[1] M.C. Cross and P.C. Hohenberg, Rev. Mod. Phys. **65**, 851 (1993).
[2] B. Billia and R. Trivedi, in *Handbook of Crystal Growth*, edited by D.T.J. Hurle (Elsevier, Amsterdam, 1993), Vol. 1, Chap. 14.
[3] M.E. Glicksman and S.P. Marsh, in *Handbook of Crystal Growth* [Ref. 2], Vol. 1, Chap. 15.
[4] D. Ablitzer, J. Phys. IV **3**, 873 (1993).
[5] Y. Wang and K. Kakimoto, J. Cryst. Growth **208**, 303 (2000); Microelectron. Eng. **56**, 143 (2001).
[6] D.P. Woodruff and A.J. Forty, Philos. Mag. **15**, 985 (1967).
[7] D.P. Woodruff, Philos. Mag. **17**, 283 (1968).
[8] J.D. Verhoeven and E.D. Gibson, J. Cryst. Growth **11**, 29 (1971); **11**, 39 (1971).
[9] H.S. Chen and K.A. Jackson, J. Cryst. Growth **8**, 184 (1971).
[10] A.V. Gorbunov, Acta Metall. Mater. **40**, 513 (1992).
[11] S.R. Coriell and G.B. McFadden, in CD-Rom: Proceeding of the Second Zermatt Workshop on Solidification Microstructures, edited by M. Rappaz and R. Trivedi. The CD-ROM can be ordered from Laboratoire de Métallurgie Physique, Ecole Polytechnique Fédérale de Lausanne, CH-1015 Lausanne, Switzerland.
[12] H. Nguyen Thi, D. Camel, Y. Dabo, B. Drevet, and B. Billia, in *Proceedings of the International Conference on The Science of Casting and Solidification* (Editura Lux Libris, Brasov, Romania, 2001), p. 60; J. Phys. IV **11**, Pr6 (2001).
[13] W.W. Mullins and R.F. Sekerka, J. Appl. Phys. **35**, 444 (1964).
[14] N. Noël, F. Zamkotsian, H. Jamgotchian, and B. Billia, Meas. Sci. Technol. **11**, 66 (2000).
[15] W.A. Tiller, J.W. Rutter, K.A. Jackson, and B. Chalmers, Acta Metall. **1**, 428 (1953).
[16] N. Noël, H. Jamgotchian, and B. Billia, J. Cryst. Growth **181**, 117 (1997); *ibid.* **187**, 516 (1998).
[17] H. Jamgotchian, N. Bergeon, D. Benielli, P. Voge, B. Billia,

and R. Guérin, Phys. Rev. Lett. **87**, 166105 (2001).
[18] Yu.V. Naidich, N.F. Grigorenko, and V.M. Perevertailo, J. Cryst. Growth **53**, 261 (1981).
[19] S. Akamatsu, G. Faivre, and T. Ihle, Phys. Rev. E **51**, 4751 (1995).
[20] N. Noël, H. Jamgotchian, and B. Billia, J. Cryst. Growth **187**, 516 (1998).
[21] J.S. Kirkaldy, L.X. Liu, and A. Kroupa, Acta Metall. Mater. **43**, 2905 (1995).
[22] W.R. Pfann, Trans. AIME **203**, 961 (1955).
[23] W.A. Tiller, J. Appl. Phys. **34**, 2757 (1963).
[24] M. Gäumann, R. Trivedi, and W. Kurz, Mater. Sci. Eng., A **226-228**, 763 (1997).
[25] K. Lu and Y. Li, Phys. Rev. Lett. **80**, 4474 (1998).
[26] J.A. Warren and J.S. Langer, Phys. Rev. E **47**, 2702 (1993).
[27] W.W. Mullins and R.F. Sekerka, J. Appl. Phys. **34**, 323 (1963).
[28] R.J. Schaeffer and M.E. Glicksman, J. Cryst. Growth **5**, 44 (1969).
[29] D.J. Allen and J.D. Hunt, in *Solidification and Casting of Metals* (Metals Society, London, 1979), p. 39.
[30] E. Brener, Phys. Rev. Lett. **71**, 3653 (1993).